# Performance Enhancement of an Ag–Au Bimetallic SPR Sensor: A Theoretical and Experimental Study

Roshni S. Babu, Hamish R. Colenso, Gideon J. Gouws, *Senior Member, IEEE*, Baptiste Auguié, and Ciaran P. Moore, *Member, IEEE*

Abstract—Ag–Au bimetallic surface plasmon resonance (SPR) sensors operating in the Kretschmann configuration were investigated by numerical modeling and experiment. While Ag-based sensors have good sensitivity, they suffer from poor stability, and the addition of an Au capping layer offers improved chemical resistance and reliable analyte bonding via thiol–gold interactions. Sensors were evaluated with an Ag–Au combined thickness of 50 nm but different thickness ratios, and SPR reflectivity curves were obtained for 632.8 nm wavelength light incident over a range of angles. Numerical modeling using the transfer matrix method showed the SPR response improving as Au thickness decreased, giving the best results for 45 nm of Ag and 5 nm of Au. Experimental characterization of fabricated Ag–Au bimetallic sensors was carried out with a custom SPR testbed. Performance parameters, including minimum reflectivity, full-width at half-maximum (FWHM), stability, and

sensitivity were measured and the results were compared to those of single-layer Ag and Au sensors. A 5 nm Au coating was unable to preserve stable bimetallic sensor performance; however, increasing the Au thickness to 10 nm was sufficient to protect the Ag sensing layer, allowing only a small variation in the minimum reflectivity and FWHM when exposed to analytes for multiple hours. The sensitivity of the single-layer Ag, bimetallic Ag–Au, and Au sensors was measured as 3041%/refractive index unit (RIU), 1817%/RIU, and 1229%/RIU, respectively. The sensitivity of the thickness-optimized bimetallic layer was ∼1.5× that of the single-layer Au sensor.

Index Terms— Bimetallic sensor, Kretschmann configuration, sensitivity, surface plasmon resonance (SPR).
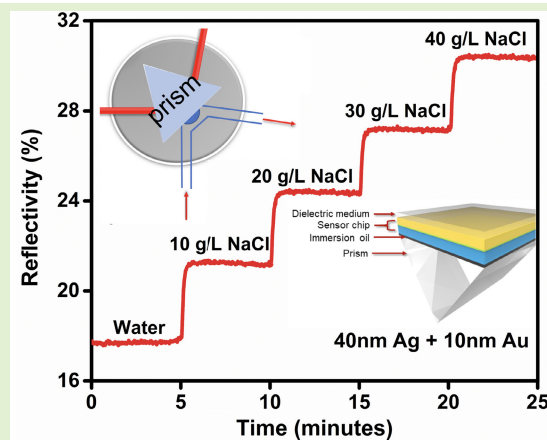
I. INTRODUCTION

SURFACE plasmon resonance (SPR) biosensors are an indispensable analytical tool for the rapid and sensitive

Roshni S. Babu was with the School of Engineering and Computer Science, Victoria University of Wellington, Wellington 6140, New Zealand. She is now with the School of Electronics and Computer Science, University of Southampton, SO17 1BJ Southampton, U.K. (e-mail: R.Satheesh-Babu@soton.ac.uk).

Hamish R. Colenso and Gideon J. Gouws are with the School of Engineering and Computer Science, Victoria University of Wellington, Wellington 6140, New Zealand (e-mail: hamish.colenso@vuw.ac.nz; gideon.gouws@vuw.ac.nz).

Baptiste Auguié is with the School of Physical and Chemical Sciences, Victoria University of Wellington, Wellington 6140, New Zealand (e-mail: baptiste.auguie@vuw.ac.nz).

Ciaran P. Moore is with the Department of Electrical and Computer Engineering, University of Canterbury, Christchurch 8140, New Zealand (e-mail: ciaran.moore@canterbury.ac.nz).

detection of chemical and biological molecules by measuring changes in refractive index in the nanoscale vicinity of the sensor chip [1]. SPR instruments have the potential to provide information about the concentration and real-time kinetic data of a biomolecular interaction, including the association and dissociation of ligands with an analyte [1], comparable to other biosensing platforms such as electrochemical [2], fluorescence [3], calorimetric [4], and quartz crystal monitors (QCMs) [5]. Applications of these sensors include medical diagnostics [6], [7], [8], [9], food control [10], and environmental monitoring [11], [12].

Au and Ag are frequent candidates for SPR sensors due to their high electrical conductivity. Ag thin film sensors tend to be more cost-effective than Au devices and produce a sharp resonance dip in their reflection spectra, which leads to higher sensitivity and signal-to-noise ratios than equivalent Au sensors when the intensity or phase of light reflected by the SPR sensor are measured to detect changes in the refractive index of an analyte [22]. However, the poor chemical stability of Ag thin films prevents their use in practical applications, as Ag corrodes in air, and the

process is accelerated in an aqueous solution [23]. On the other hand, Au sensors produce a larger shift in resonant angle as analyte refractive index changes [25], making them better suited to sensing schemes that sweep the wavelength or angle of the incoming light. Au also has good chemical resistance, better stability, and higher thiol affinity than Ag [24], making it the preferred option in many commercial systems.

Several attempts have been made to improve the sensitivity and robustness of Ag and Au SPR sensors: plasmonic structures, such as metal nanoparticles [13], metallic nanoslits [14], nanoholes [15], colloidal Au nanoparticles [16], 2-D nanomaterials [17], and multilayer structures [18] have been successfully explored as the sensing layer to improve sensitivity. However, better performance was realized only at the cost of increased complexity of optical configuration and sensor chip fabrication. Recently, significant efforts have been taken to develop different multilayer structures instead of a single planar Au layer sensor chip [19], [20], [21]. Multilayer planar structures are relatively easy to fabricate and can be easily measured using the same SPR measurement setup used for single-layer chips, avoiding additional complexity in the SPR instrumentation.

Different multilayer approaches have evolved so far to utilize the optical properties of Ag by providing a thin and dense protective layer by the use of materials such as Au [26], [27], [28], dielectrics [29], [30], or self-assembled monolayers [31]. The first experimental application of bimetallic Ag–Au layers for SPR sensing was carried out in 1995 [32]. Subsequent theoretical reports discussed different methods to improve the sensitivity of bimetallic SPR sensors [27], [33], [34], [35], [36], [37], [38], [39], [40]. In 2002, Wu and Ho numerically analyzed an Ag–Au bimetallic SPR sensor using Fresnel's equations and found that thicknesses of 48 nm Ag and 2 nm Au gave the best performance [34].

Several other reports are available for Ag–Au bimetallic sensors [27], [33], [35], [38], [40]; however, only a few use the intensity interrogation method [33], [35]. Alieva and Konopsky [35] performed experiments on Ag–Au bimetallic layers in a real biosensor system, using phase interrogation. Ong et al. [27], with the support of analytical calculation using the transfer matrix method, investigated the SPR responses of Ag–Au bimetallic sensors experimentally using the angular interrogation method. Wang et al. [38] fabricated a bimetallic Ag–Au sensor and obtained a maximum sensitivity of 5250%/refractive index unit (RIU) in Milli-Q water analyte using the intensity interrogation method. Prabowo et al. [40] demonstrated the applicability of a white LED source operating at two different wavelengths (510 and 580 nm) in measuring the SPR response of an Ag–Au bimetallic layer and obtained a high sensitivity of 4859%/RIU; however, stability was not discussed in their work. Despite several theoretical studies of Ag–Au bimetallic SPR sensors over the past two decades [4], [13], experimental studies have largely avoided the question of stability of Ag–Au bimetallic SPR sensors in a corrosive atmosphere.
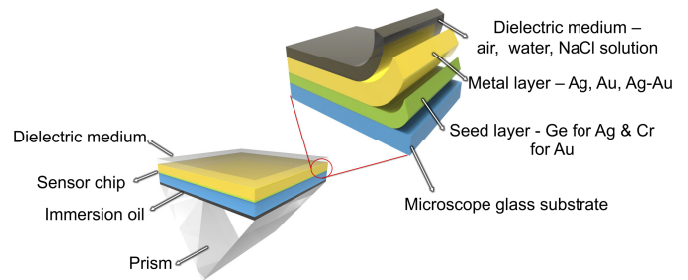

Fig. 1. Schematic of the bimetallic SPR sensor. Immersion oil ensures good optical contact between the BK7 prism and the glass slide. Due to the poor adhesion of Ag and Au with the glass, a very thin (∼2 nm) adhesion layer (seed layer) is used between glass and metal. Ge is used as the seed layer for Ag and Cr for Au. Air, water, and sodium chloride (NaCl) solutions are used as the analyte media.

This article reports a systematic analytical and experimental study of Ag–Au bimetallic SPR sensor chips based on the intensity interrogation method. First, the transfer matrix method was used to optimize the thickness of the Ag and Au films in the bimetallic structure. High-performance Ag–Au bimetallic sensor chips, shown in Fig. 1, were then fabricated, and the sensitivity and chemical stability of these Ag–Au sensor chips were measured using a custom SPR testbed.

II. ANALYTICAL MODELING

The SPR sensor chip was modeled as a five-layer system consisting of: 1) a semi-infinite Schott BK7 glass layer, representing a prism, microscope slide substrate, and refractive index matching oil that ensured optical homogeneity between them; 2) a germanium (Ge) or chromium (Cr) seed layer; 3) the Ag sensing layer; 4) the Au capping layer; and 5) a semi-infinite analyte layer, which was either air, water, or NaCl solution. Specifying semi-infinite layers at the extremes of the model allowed a 1-D model to be used, which was able to produce helpful results without the need to consider the dependence of the prism thickness on beam position nor the geometry of the analyte channel. In our previous work, we determined that a total metallic thickness of 50 nm demonstrated optimum SPR performance [41], in the form of very low SPR minimum reflectance, as shown in Fig. S1. Therefore, we designed our bimetallic system to have a total thickness of 50 nm between Ag and Au. The material properties of different layers used for modeling are given in Table I.

The reflectivity of an ideal SPR sensor can be calculated by considering the optical impedance mismatch between individual planar layers within the sensor. In the simplest case of a sensor comprising only an interface between two semi-infinite layers, the reflectivity R at wavelength λ_0 and angle of incidence θ is determined by the contrast [48] between optical impedances, Z_m, of the two layers. R of the system is given by the following equation [49]:

$$R = \left| \frac{Z_1 - Z_0}{Z_1 + Z_0} \right|^2 \qquad (1)$$

where $Z_m = (k_{m,z}/\epsilon_m k_0)$, with $k_{m,z} = (\epsilon_m k_0^2 - k_\parallel^2)^{1/2}$ and $k_\parallel = k_0 \sqrt{\epsilon_0} \sin\theta$ for TM polarization [49]. Here ϵ_m is

TABLE I
PARAMETERS FOR SENSORS MODELED IN THIS WORK

Layer, m	Material	Relative permittivity at 632.8 nm wavelength, ϵ_m	Thickness, d	Physical equivalent
0	BK7 glass	2.2955 [42]	semi-infinite	substrate
1	Ge	$10.7057 + 2.7177i$ [43]	2 nm	seed layer
1	Cr	$-7.0107 + 29.858i$ [44]	2 nm	seed layer
2	Ag	$-18.644 + 0.44275i$ [45]	{50, 45, 40, 30, 20, 10, 0} nm	plasmonic film
3	Au	$-13.013 + 1.0331i$ [45]	50 nm$-d_{Ag}$	plasmonic film
4	Air	1.0006 [46]	semi-infinite	sensing medium
4	Water	1.7818 [47]	semi-infinite	sensing medium
4	NaCl	$1.7865 - 1.8010$ [47]	semi-infinite	sensing medium

the (complex) relative permittivity of the layer, $k_0 = (2\pi/\lambda_0)$ is the free space wavenumber, $k_\parallel = k_0\sqrt{\epsilon_0}\sin\theta$ is the wavenumber of light in the plane of the interface, and $k_{m,z}$ is the component of the wavevector normal to the interface, i.e., in the direction of propagation of the incident light.

Extending this model to systems with more than two layers means considering not just the contrast between the impedances of the first two layers but between the impedance of the first layer and the input impedance, Z_{in}, presented by the next layer and every subsequent layer. The input impedance for the mth layer is defined recursively by

$$Z_{in,m} = Z_m \left[\frac{Z_{in,m+1} - iZ_m \tan\left(k_{m,z}d_m\right)}{Z_m - iZ_{in,m+1}\tan\left(k_{m,z}d_m\right)} \right] \quad (2)$$

where the input impedance for the final layer in the sensor, $Z_{in,M-1}$, reduces to Z_{M-1}. Here d_m is the thickness of the mth layer; the thickness of the final layer is assumed to be semi-infinite. Working backwards from $m = M-1$ to $m = 0$ allows R to be calculated for the complete sensor [49], [50].

Finding authoritative data for the refractive index of NaCl aqueous solution under conditions that matched our experimental setup proved to be challenging. Several papers report values at the wavelength (632.8 nm) and over the range of concentrations (0–40 g/L) we are using [51]; however, they do not consider the effect of temperature. As a result, there is some variation in the refractive indices they report. Papers that consider temperature either use a different wavelength (589.3 nm) [47] or consider a much broader range of concentrations [52], with very few data points in our range of interest. To avoid overstating the sensitivity of the sensors reported here, we calculate refractive indices based on the empirical equations derived in [47], which give the largest variation in refractive index values over the range of concentrations that we consider.

The refractive index, n of different concentrations of NaCl solution at a wavelength of 632.8 nm and a temperature T of 291.15 K were obtained according to (3) [47] at the concentrations given in Table II. The concentration, C in (3)

TABLE II
REFRACTIVE INDEX OF NaCl AQUEOUS SOLUTION AT A WAVELENGTH OF 632.8 NM AND TEMPERATURE OF 291.15 K

Concentration, C (g/L)	Refractive index, n
0	1.3348
10	1.3366
20	1.3384
30	1.3402
40	1.3418

is in (kg/kg) $\times 100 \approx$ (g/L) $\div 10$.

$$n = 1.3373 + (1.7682 \times 10^{-3})C - (5.8 \times 10^{-6})C^2$$
$$- (1.3531 \times 10^{-4})(T - 273.15)$$
$$- (5.1 \times 10^{-8})(T - 273.15)^2. \quad (3)$$

III. EXPERIMENTAL MATERIALS AND METHODS

To verify the theoretical calculations, bimetallic and single-layer sensors were fabricated with Ag and Au as sensing layers. Ge was used as a seed layer below Ag films to reduce the roughness of the Ag films [53], which results in a stronger plasmon resonance [54], while Cr was used to improve adhesion [55] in Au-only sensors. The schematic of an Ag–Au bimetallic SPR sensor working in the Kretschmann configuration is depicted in Fig. 1.

Sample preparation started with cleaning the microscope glass substrates using piranha solution (3 H_2SO_4:1 H_2O_2). The piranha-cleaned substrates were washed with distilled water and dried with compressed N_2 gas. Materials for seed layers (Cr and Ge), and metal layers (Ag and Au), obtained from Kurt J Lesker, USA, were deposited on the glass substrates at a pressure of $\sim 1.1 \times 10^{-6}$ torr and a deposition rate of 0.1 Å/s using a thermal evaporator (Angstrom Engineering Nexdep 200, Canada). The thickness of the deposited thin films was characterized using a surface profilometer (Veeco Dektak-150, USA). Optical contact between the metal-coated glass slide and the 45° BK7 prism was obtained using a refractive index matching oil (immersion oil type F, Olympus, Thorlabs, USA). Different concentrations of NaCl (Sigma Aldrich, New Zealand) in distilled water were used for sensitivity analysis.

A. Sensor Characterization

A schematic and photograph of the characterization testbed [41] based on the Kretschmann configuration are shown in Fig. 2. A monochromatic He-Ne laser (Melles Griot part number 05-LHP-121) emitted red light of 632.8 nm wavelength at 2.0 mW nominal output power through two irises and a polarizer (Thorlabs part number CCM5-BS016/M). The transmitted p-polarized light was then split into two perpendicular beams by a nonpolarizing beam splitter cube. After splitting, one of the light beams was directed into photodetector 1. This was taken as the reference beam. The other light beam was guided to the BK7 prism with the help of two mirrors. The second photodetector captured the reflected light from the prism. The reflectivity data were normalized by dividing the reflected light intensity by the reference light intensity. To change the angle of incidence, the prism and its

TABLE III
MODELED (SIM) AND MEASURED (EXP) RESONANT ANGLE (θ) AND FWHM OF SINGLE-LAYER
AND BIMETALLIC AG AND AU SENSORS IN AIR AND WATER

| Configuration		Air				Water				Change from Air to Water
		θ_{sim} (deg)	θ_{exp} (deg)	$FWHM_{sim}$ (deg)	$FWHM_{exp}$ (deg)	θ_{sim} (deg)	θ_{exp} (deg)	$FWHM_{sim}$ (deg)	$FWHM_{exp}$ (deg)	$\Delta\theta_{exp}$ (deg)
50 nm	Ag	42.78	42.98	0.20	0.77	67.58	67.65	0.86	1.77	24.67
45-5 nm	Ag-Au	42.98	43.19	0.30	1.07	68.53	68.67	1.39	3.35	25.48
40-10 nm	Ag-Au	43.13	43.34	0.37	1.17	69.14	69.15	1.83	4.4	25.81
30-20 nm	Ag-Au	43.32	43.41	0.50	1.24	70.10	70.55	2.50	5.3	27.14
20-30 nm	Ag-Au	43.42	43.54	0.62	1.31	70.55	71.25	2.99	5.9	27.71
10-40 nm	Ag-Au	43.48	43.61	0.74	1.43	70.76	71.85	3.42	6.5	28.24
50 nm	Au	43.56	43.82	1.05	1.68	70.91	72.49	3.66	7.1	28.67

(a)

(b)
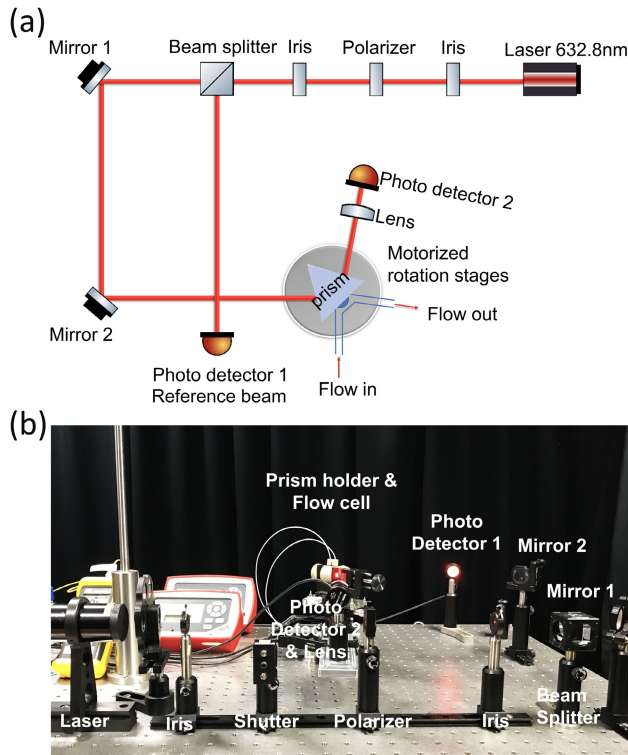
Fig. 2. (a) Schematic and (b) photograph of the experimental setup used for SPR sensor characterization.

associated parts (including the glass slide, metallic coating, and microfluidic flow cell) were mounted on a motorized stage (Thorlabs part number PRMTZ8/M) and rotated with respect to the stationary light source. Photodetector 2 and a focusing lens were mounted on a second rotary stage (Thorlabs PRMTZ8/M), which was coaxial with the first stage and rotated at the same rate but in the opposite direction to the prism. The experimental testbed was automated, and data recording was done using LabVIEW 2018 software. A peristaltic pump system (Mitos P-Pump, Dolomite, U.K.) was used to circulate solutions through the flow cell attached to the sensor chip at a flow rate of approximately 50 μL/min. Measurements were taken at an ambient temperature of 18 °C.

IV. RESULTS AND DISCUSSION

Theoretical and experimental reflectivity curves for Ag–Au bimetallic SPR sensors in air and water are plotted in Fig. 3.

Curves for single-layer Ag and Au thin films are also shown to facilitate direct comparison. A detailed comparison between the numerical values of calculated and measured data for different configurations in air and water is presented in Table III.

The minimum reflectivity point in the SPR response curve is due to the absorption resulting from the maximum coupling between the electric fields of the incident light and the surface plasmons [10]. The incidence angle at which the reflectance minimum occurs, which corresponds to the resonant angle calculated by our model, is observed at 42.98° for a single-layer Ag sensor and 43.82° for a single-layer Au sensor, both in air. In water, the resonant angles of single-layer Ag and Au sensors increased to 67.65° and 72.49°, respectively, due to the higher refractive index of water ($n \approx 1.3348$) compared to air ($n \approx 1.003$). The resonant angles of all the examined thickness combinations of Ag–Au bimetallic sensors lie between those of single-layer Ag and Au in both air and water, and are listed in Table III.

These experimental data were in good qualitative agreement with the modeled results, showing the same trends of increasing resonance angle and broadened reflectivity curve as the proportion of Au in the sensor was increased. The data differed quantitatively in two key aspects: both the measured reflected intensities and the sharpness of the sensor responses, determined by the full-width at half-maximum (FWHM) of the reflectivity spectra, were lower than predicted by the model. Both of these discrepancies can be traced to nonzero beam divergence: the lower-than-expected intensities resulted from a greater path length to the measurement photodetector, photodetector 2 in Fig. 2, than the reference detector, photodetector 1, which meant that the beam had more time to diverge traveling to photodetector 2 than it did to photodetector 1, resulting in lower intensities measured at photodetector 2 even before a sensor was introduced. Similarly, divergence in the beam through the prism meant that the sensor was always interrogated at a range of angles simultaneously, leading to an increased FWHM compared to the ideal, modeled case. This FWHM broadening was consistent with observations in other experimental studies [49]. Despite these differences, the qualitative consistency of results between the experimental testbed and the model allow the design of a bimetallic sensor to be explored and refined.

For both air and water, the FWHM of the reflected intensity with respect to the angle of incidence is the smallest for Ag, increasing with the thickness of the Au layer. This is favorable
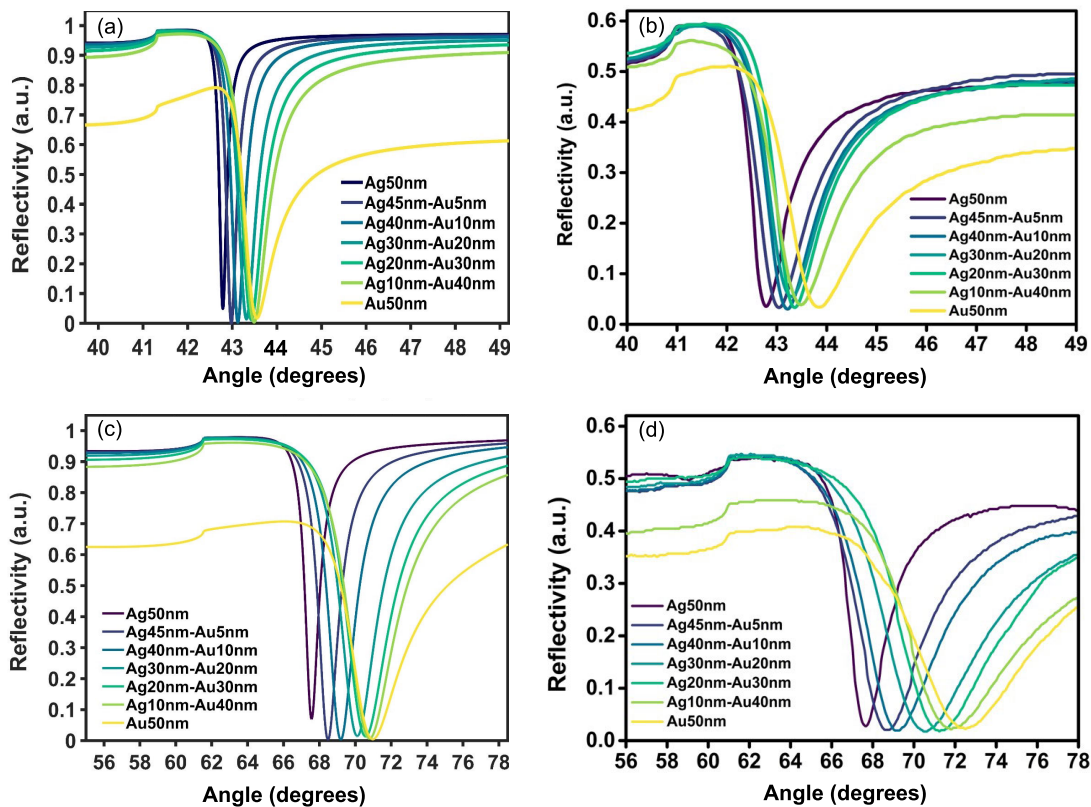
Fig. 3. (a) and (c) Simulated and (b) and (d) experimental reflectivity curves of single-layer Ag, Au, and bimetallic Ag–Au configurations in (a) and (b) air and (c) and (d) water.

for sensing using intensity interrogation but it introduces a compromise: thicker Au increases the chemical robustness and stability of the thin films; however, it also adversely affects the FWHM of reflected intensity. The higher the thickness of Au, the greater the broadening effect. This broadening is attributed to the intrinsic damping of surface plasmons contributed by the large imaginary part of the dielectric constant of Au [56]. Conversely, the change in resonant angle when moving from air to water, in other words, the change in resonant angle for a given change in refractive index, increased with increasing Au thickness, which would be beneficial in an angle interrogation sensing regime. In summary, Fig. 3(b) and (d) show a near-zero reflectivity and narrow FWHM for Ag–Au bilayer thicknesses of 45–5 nm and 40–10 nm in air and water. At this stage, it was necessary to confirm whether a 5 nm Au layer was sufficient to give stable sensor performance.

A. Sensor Stability

In a typical biosensing experiment [6], [10], [11], both the biological element and analytes are dissolved in a buffer solution, often a salt solution. Therefore, the sensor layer, which is in direct contact with the salt solution, must be chemically stable. Au is reported to have better chemical stability than Ag in various reactive chemical environments [22], hence in this experiment we used an Au capping layer as a protective layer for Ag, with different Au and Ag layer thickness combinations. We studied the influence of the capping layer on the chemical stability of the sensor when immersed in a salt solution.

To check the stability, sensor chips were kept in a 2 w/w% solution of NaCl in distilled water for 12 h. The reflectance spectra of the chips were measured periodically, as shown in Fig. 4. Ag sensors without any capping layer and 5 nm Au capping layer experienced huge variations in minimum reflectivity and FWHM as time progressed. This suggests that a 5 nm Au layer is insufficient for protecting the inner Ag against the corrosion induced by the salt ions, where chloride ions from the salt oxidize Ag to form AgCl according to the chemical reaction

$$Ag + Cl^- \rightleftharpoons AgCl + e^-. \tag{4}$$
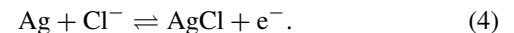
The thickness of the AgCl film will increase gradually as the exposure time increases [57], [58]. Since Au has the highest standard electrode potential of 1.38 V, it is widely used for plating due to its high corrosion resistance [59]. It has fair corrosion resistance in a chloride environment. Moreover, the efficiency of the Au layer in protecting the underlying surface against the attack of corroding material is determined by the uniformity of the Au layer. In general, more uniform layers are obtained at higher thicknesses. Very thin layers of Au are known to be porous [60], hence providing poor protection against corrosion. Fig. 4(b) shows that the sensors with a 5 nm thick Au layer are not able to hold their stability in the NaCl solution for many hours, which suggests nonuniformity in the Au protective layer. The 5 nm protective layer did not provide effective coverage to the underlying Ag, leading to
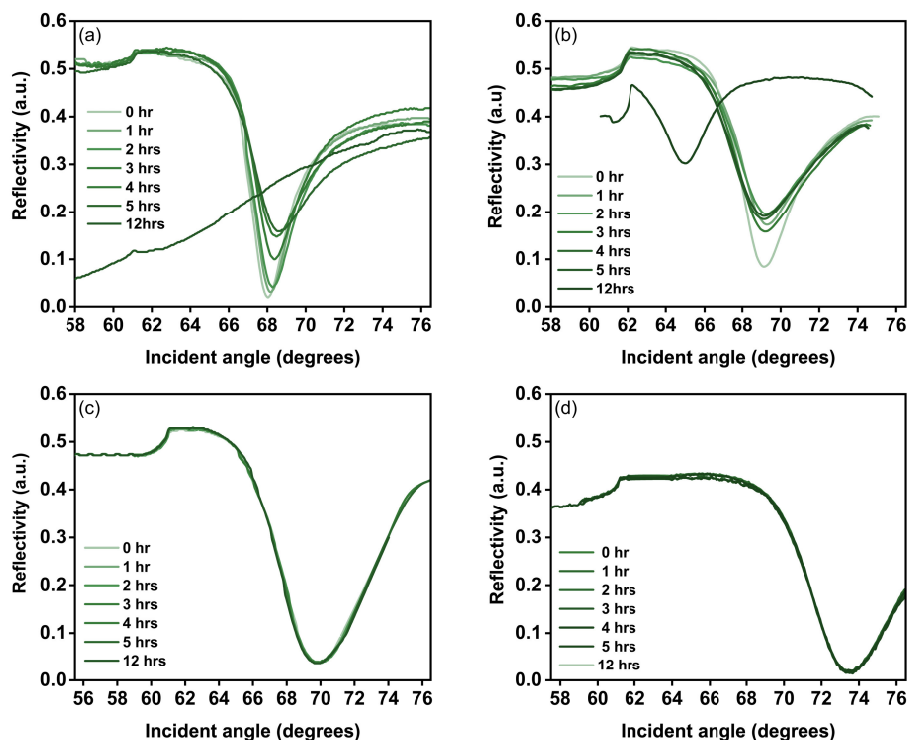
Fig. 4. Stability test of (a) 50 nm Ag single-layer sensor, (b) 45–5 nm Ag–Au bimetallic sensor, (c) 40–10 nm Ag–Au bimetallic sensor, and (d) 50 nm Au single-layer sensor, all kept in contact with 2 w/w% NaCl solution for up to 12 h.
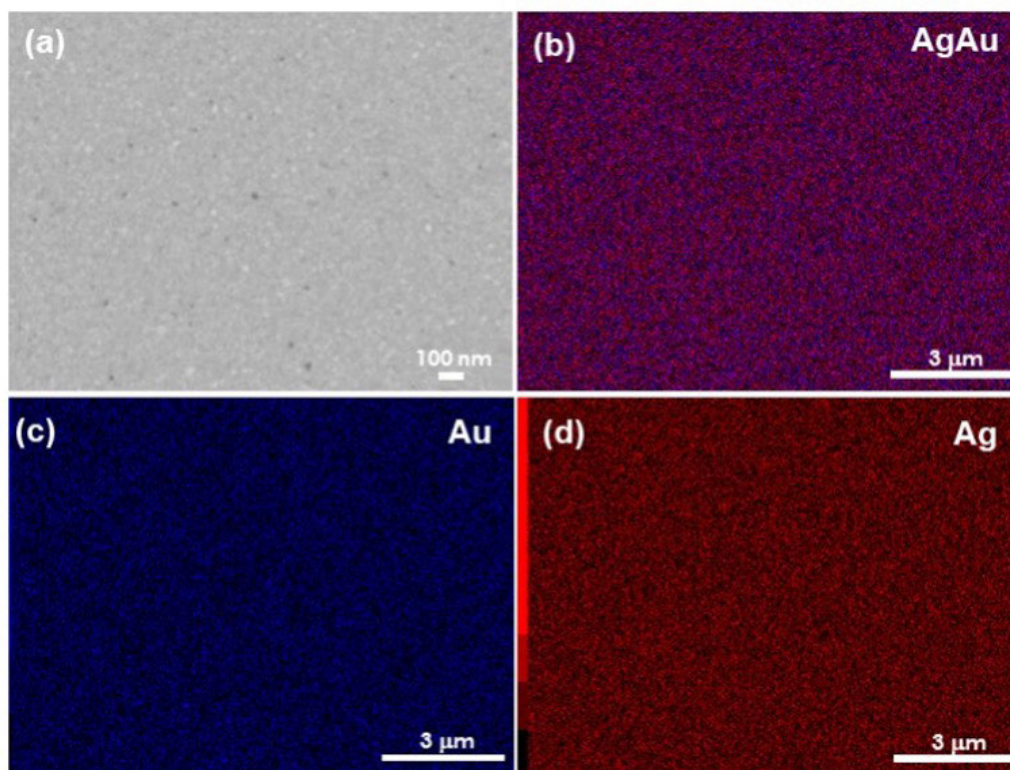

Fig. 5. (a) Scanning electron micrograph of a 40–10 nm Ag–Au bimetallic thin film surface. (b)–(d) Elemental color mappings for the film shown in (a), with (b) and (c) Au mapped to blue and (b) and (d) Ag mapped to red.

Ag deterioration and resulting in inefficient SPR excitation, which worsened as time progressed.

This hypothesis of poor coverage at lower Au thickness is complemented by the SPR analysis of an Ag film with 10 nm Au capping layer, shown in Fig. 4(c). At this thickness, the sensor showed a highly stable response in the salt solution for over 12 h, confirming the chemical stability of the bimetallic chip. Hence, we chose 10 nm of Au and 40 nm of Ag as the
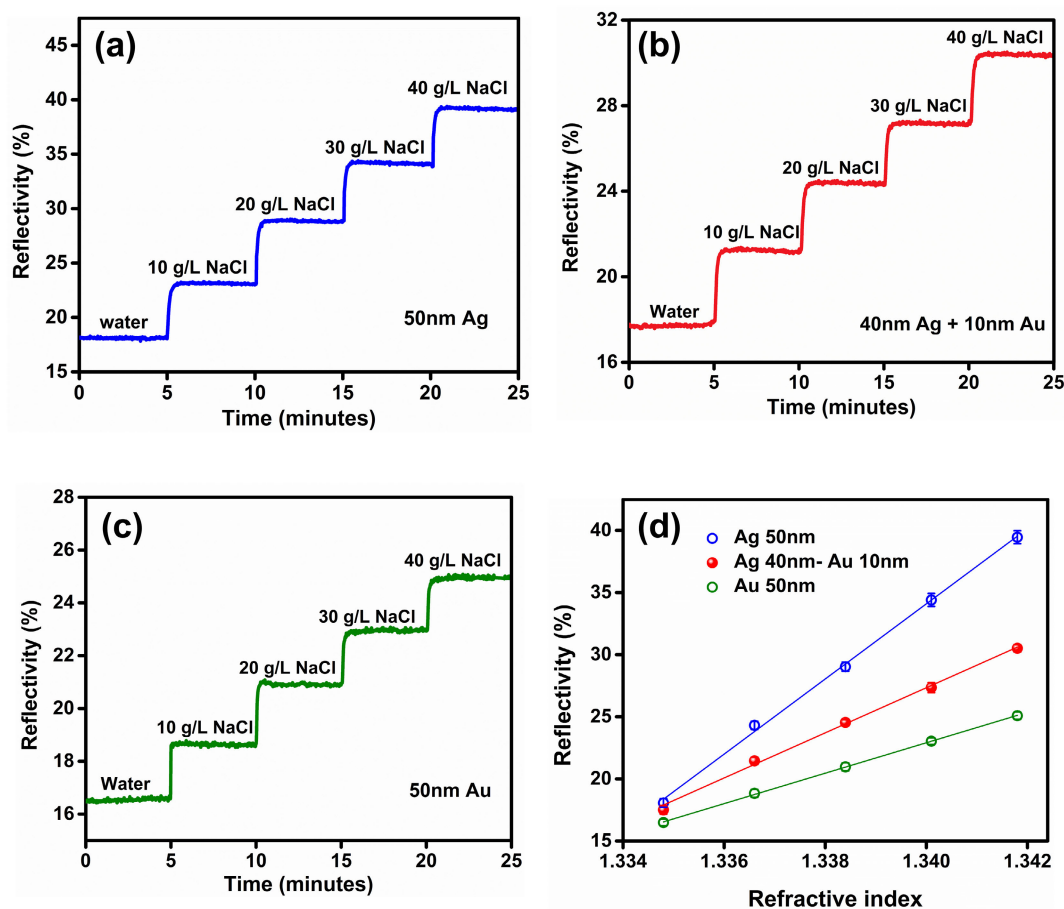
Fig. 6. Sensitivity studies of (a) 50 nm Ag single-layer sensor, (b) 40–10 nm Ag–Au bimetallic sensor, and (c) 50 nm Au single-layer sensor. Calculating the refractive index expected at each NaCl concentration gives the sensor sensitivity curves shown in (d).

optimized thickness for this structure. Further stability studies of different thicknesses of Ag and Au films are shown in Fig. S2. All the sensors with at least 10 nm of Au successfully survived the salt solution test. We note here that optimization of the metal deposition process, or use of an alternative deposition technique, may well allow thinner capping layers that still offer sufficient protection to Ag-based sensors.

B. Film Uniformity

Surface and elemental mapping images for a bimetallic film with 10 nm Au coating over a 40 nm thick Ag layer are shown in Fig. 5. Fig. 5(a) shows the surface of the bimetallic film, while Fig. 5(b)–(d) show color mappings corresponding to Ag (red) and Au (blue). The uniformity of the Au film, shown in Fig. 5(c), explains the improved stability seen in Fig. 4, while the strong Ag signal shown in Fig. 5(b) and (d) is most likely due to the large penetration depth of the imaging electrons relative to the thickness of the Au film [61]. Further evidence for the integrity of the Au film is in the form of energy dispersive X-ray spectrography, shown in Fig. S3, which demonstrates much higher relative abundance of Au compared to Ag, Ge, and Si on the bilayer surface.

C. Sensitivity

Sensitivity can be found either by measuring the incident angle that gives minimum reflectivity or by measuring the change in reflectivity at a fixed incident angle. Here we adopted the fixed angle method, choosing the angle that corresponds to the highest slope in the SPR response curve for distilled water. This slope can be measured much more accurately than the angle of minimum reflectivity because it is approximately constant over a range of incident angles. Fig. 6(a)–(c) show the real-time responses of single layers and bimetallic layers of Ag and Au over a short period of time. The fixed angles used for measurement are obtained from the maximum of the first derivative of the SPR curves shown in Fig. 3(d). These angles are 70.4°, 66.9°, and 68.1° for single-layer Au, Ag, and a 40–10 nm Ag–Au bimetallic layer, respectively. Distilled water was used as the baseline and, once the signal was stabilized, NaCl solutions with concentrations of 10, 20, 30, and 40 g/L were injected at a flow rate of 50 μL/min. The solution concentration was increased every 5 min. As the refractive index of the NaCl solution, calculated using (3), increases with concentration, an increase in reflected intensity is observed, shown in Fig. 6(d). The sensitivity, S of the system can be calculated from the rate of change of

reflectivity, R with n [66]:

$$S = \frac{dR}{dn}. \tag{5}$$

The sensitivity of the Ag, Au, and bimetallic Ag–Au SPR sensors was calculated as 3041%/RIU, 1229%/RIU, and 1817%/RIU, respectively.

D. Surface Roughness

While the differences in sensitivity for sensors shown in Fig. 6 are readily explained by metallic film composition, the surface roughness of the metal films can also play some role [62], [63], [64], but not for surface roughness below 2 nm$_{rms}$ [65]. For this reason the surface roughness of each metallic film was measured via atomic force microscopy; typical results were 0.86 nm$_{rms}$ for the 50 nm Ag films, 1.95 nm$_{rms}$ for the 40–10 nm Ag–Au bilayers, and 2.09 nm$_{rms}$ for the 50 nm Au films (see Fig. S4). These low roughness values for Ag films are evidence of ultra-smooth metallic surfaces that are unlikely to hinder sensor performance; for the bimetallic and Au films, the possibility of better sensitivity via decreased surface roughness may exist but is far from certain.

V. CONCLUSION

This article demonstrates a bimetallic Ag–Au SPR sensor chip with better sensitivity than Au-only sensors and better stability compared to Ag-only sensors. The SPR response curves for single-layer Ag, Au, and bimetallic Ag–Au layers were obtained. Based on the experimental and simulated results, the performance parameters of the chips were evaluated, and after thorough comparison, a bimetallic sensor chip with 40 nm of Ag with a 10 nm Au capping layer was selected as the optimum design. The sensitivity of the bimetallic sensor chip was improved compared to a single-layer Au sensor, without any of the durability concerns of an Ag sensor. These findings facilitate the continued development of SPR-based sensors for high-resolution applications where expected refractive index changes are particularly small, such as in waterways contaminated with agricultural runoff [67] or open-air environmental monitoring stations [11].

REFERENCES

[1] R. B. M. Schasfoort, *Handbook of Surface Plasmon Resonance*, 2nd ed. Cambridge, U.K.: Royal Society of Chemistry, 2017.

[2] B. Bansod, T. Kumar, R. Thakur, S. Rana, and I. Singh, "A review on various electrochemical techniques for heavy metal ions detection with different sensing platforms," *Biosensors Bioelectron.*, vol. 94, pp. 443–455, Aug. 2017.

[3] Y. Jeong, Y.-M. Kook, K. Lee, and W.-G. Koh, "Metal enhanced fluorescence (MEF) for biosensors: General approaches and a review of recent developments," *Biosensors Bioelectron.*, vol. 111, pp. 102–116, Jul. 2018.

[4] A. Halilovic, E. Merdan, Z. Kovacevic, and L. G. Pokvic, "Review of biosensors for environmental field monitoring," in *Proc. 8th Medit. Conf. Embedded Comput. (MECO)*, Jun. 2019, pp. 1–8.

[5] S. Seif, T. Thundert, and K. Cadien, "Review on ultra-sensitive QCM mass sensor and microfluidic for diagnostic point of care," *Sensors Transducers J.*, vol. 215, no. 8, pp. 1–7, Aug. 2017.

[6] J.-F. Masson, "Surface plasmon resonance clinical biosensors for medical diagnostics," *ACS Sensors*, vol. 2, no. 1, pp. 16–30, Jan. 2017.

[7] V. S. Chaudhary, D. Kumar, and S. Kumar, "Gold-immobilized photonic crystal fiber-based SPR biosensor for detection of malaria disease in human body," *IEEE Sensors J.*, vol. 21, no. 16, pp. 17800–17807, Aug. 2021.

[8] V. S. Chaudhary, D. Kumar, G. P. Mishra, S. Sharma, and S. Kumar, "Plasmonic biosensor with gold and titanium dioxide immobilized on photonic crystal fiber for blood composition detection," *IEEE Sensors J.*, vol. 22, no. 9, pp. 8474–8481, May 2022.

[9] V. S. Chaudhary, D. Kumar, and S. Kumar, "Au-TiO$_2$ coated photonic crystal fiber based SPR refractometric sensor for detection of cancerous cells," *IEEE Trans. Nanobiosci.*, early access, Nov. 3, 2022, doi: 10.1109/TNB.2022.3219104.

[10] J. Zhou et al., "Surface plasmon resonance (SPR) biosensors for food allergen detection in food matrices," *Biosensors Bioelectron.*, vol. 142, Oct. 2019, Art. no. 111449.

[11] A. I. Mahmood, R. K. Ibrahim, A. I. Mahmood, and Z. K. Ibrahim, "Design and simulation of surface plasmon resonance sensors for environmental monitoring," *J. Phys., Conf. Ser.*, vol. 1003, May 2018, Art. no. 012118.

[12] G. P. Mishra, D. Kumar, V. S. Chaudhary, and S. Kumar, "Design and sensitivity improvement of microstructured-core photonic crystal fiber based sensor for methane and hydrogen fluoride detection," *IEEE Sensors J.*, vol. 22, no. 2, pp. 1265–1272, Jan. 2022.

[13] B. Špačková, P. Wrobel, M. Bocková, and J. Homola, "Optical biosensors based on plasmonic nanostructures: A review," *Proc. IEEE*, vol. 104, no. 12, pp. 2380–2408, Dec. 2016.

[14] Z. Zeng et al., "Protein trapping in plasmonic nanoslit and nanoledge cavities: The behavior and sensing," *Anal. Chem.*, vol. 89, no. 10, pp. 5221–5229, May 2017.

[15] Y. Zhang et al., "Highly selective and sensitive probes for the detection of Cr (VI) in aqueous solutions using diglycolic acid-functionalized Au nanoparticles," *RSC Adv.*, vol. 9, no. 19, pp. 10958–10965, Apr. 2019.

[16] M. E. Stewart et al., "Nanostructured plasmonic sensors," *Chem. Rev.*, vol. 108, no. 2, pp. 494–521, Feb. 2008.

[17] A. K. Sharma and J. Gupta, "Simulation and comprehensive analysis of fluoride fiber SPR sensor with multilayer variants of 2D materials (graphene and MoS$_2$) under optimum radiation damping in NIR," *IEEE Sensors J.*, vol. 19, no. 19, pp. 8775–8780, Oct. 2019.

[18] A. Cherifi and B. Bouhafs, "Potential of SPR sensors based on multilayer interfaces with gold and LHM for biosensing applications," *Photon. Sensors*, vol. 7, no. 3, pp. 199–205, Jun. 2017.

[19] Y. Singh, M. K. Paswan, and S. K. Raghuwanshi, "Sensitivity enhancement of SPR sensor with the black phosphorus and graphene with bi-layer of gold for chemical sensing," *Plasmonics*, vol. 16, no. 5, pp. 1781–1790, Apr. 2021.

[20] M. Moznuzzaman, M. R. Islam, and I. Khan, "Effect of layer thickness variation on sensitivity: An SPR based sensor for formalin detection," *Sens. Bio-Sens. Res.*, vol. 32, Jun. 2021, Art. no. 100419.

[21] P. Varasteanu and M. Kusko, "A multi-objective optimization of 2D materials modified surface plasmon resonance (SPR) based sensors: An NSGA II approach," *Appl. Sci.*, vol. 11, no. 10, p. 4353, May 2021.

[22] S. Szunerits, X. Castel, and R. Boukherroub, "Surface plasmon resonance investigation of silver and gold films coated with thin indium tin oxide layers: Influence on stability and sensitivity," *J. Phys. Chem. C*, vol. 112, no. 40, pp. 15813–15817, Oct. 2008.

[23] G. T. Burstein. (2019). *The Tarnishing Conundrum of Silver*. Accessed: Apr. 25, 2022. [Online]. Available: https://www.assayofficelondon.co.uk/media/2566/the-tarnishing-conundrum-of-silver-g-tim-burstein.pdf

[24] C. Vericat, M. E. Vela, G. Benitez, P. Carro, and R. C. Salvarezza, "Self-assembled monolayers of thiols and dithiols on gold: New challenges for a well-known system," *Chem. Soc. Rev.*, vol. 39, pp. 1805–1834, May 2010.

[25] J. B. Maurya and Y. K. Prajapati, "A comparative study of different metal and prism in the surface plasmon resonance biosensor having MoS$_2$-graphene," *Opt. Quantum Electron.*, vol. 48, no. 5, p. 280, May 2016.

[26] S. Chen and C. Lin, "High-performance bimetallic film surface plasmon resonance sensor based on film thickness optimization," *Optik*, vol. 127, no. 19, pp. 7514–7519, Oct. 2016.

[27] B. H. Ong, X. Yuan, S. C. Tjin, J. Zhang, and H. M. Ng, "Optimised film thickness for maximum evanescent field enhancement of a bimetallic film surface plasmon resonance biosensor," *Sens. Actuators B, Chem.*, vol. 114, no. 2, pp. 1028–1034, Apr. 2006.

[28] K. M. Byun and S. H. Choi, "Investigation on an application of silver substrates for sensitive surface plasmon resonance imaging detection," *J. Opt. Soc. Amer. A, Opt. Image Sci.*, vol. 27, no. 10, pp. 2229–2236, Oct. 2010.

[29] C. Lin and S. Chen, "Theoretical investigation of detection accuracy of surface plasmon resonance sensor with dielectric layer," *J. Nanophoton.*, vol. 11, no. 4, Nov. 2017, Art. no. 046014.

[30] J. B. Maurya and Y. K. Prajapati, "Influence of dielectric coating on performance of surface plasmon resonance sensor," *Plasmonics*, vol. 12, no. 4, pp. 1121–1130, Aug. 2016.

[31] G. Wang, C. Wang, R. Yang, W. Liu, and S. Sun, "A sensitive and stable surface plasmon resonance sensor based on monolayer protected silver film," *Sensors*, vol. 17, no. 12, p. 2777, Nov. 2017.

[32] T. T. Ehler and L. J. Noe, "Surface plasmon studies of thin silver/gold bimetallic films," *Langmuir*, vol. 11, no. 10, pp. 4177–4179, Oct. 1995.

[33] S. A. Zynio et al., "Bimetallic layers increase sensitivity of affinity sensors based on surface plasmon resonance," *Sensors*, vol. 2, no. 2, pp. 62–70, 2002.

[34] S. Y. Wu and H. P. Ho, "Sensitivity improvement of the surface plasmon resonance optical sensor by using a gold-silver transducing layer," in *Proc. IEEE Hong Kong Electron Devices Meeting*, Jan. 2002, pp. 63–68.

[35] E. V. Alieva and V. N. Konopsky, "Biosensor based on surface plasmon interferometry independent on variations of liquid's refraction index," *Sens. Actuators B, Chem.*, vol. 99, no. 1, pp. 90–97, Apr. 2004.

[36] L. Xia, S. Yin, H. Gao, Q. Deng, and C. Du, "Sensitivity enhancement for surface plasmon resonance imaging biosensor by utilizing gold–silver bimetallic film configuration," *Plasmonics*, vol. 6, no. 2, pp. 245–250, Jun. 2011.

[37] C.-T. Li, K.-C. Lo, H.-Y. Chang, H.-T. Wu, J. H. Ho, and T.-J. Yen, "Ag/Au bi-metallic film based color surface plasmon resonance biosensor with enhanced sensitivity, color contrast and great linearity," *Biosensors Bioelectron.*, vol. 36, no. 1, pp. 192–198, Jun. 2012.

[38] F. Wang et al., "Sensitive surface plasmon resonance biosensor based on a photonic crystal and bimetallic configuration," in *Proc. 14th Int. Conf. Numer. Simulation Optoelectron. Devices*, Sep. 2014, pp. 117–118.

[39] Z. Wang et al., "Stable and sensitive silver surface plasmon resonance imaging sensor using trilayered metallic structures," *Anal. Chem.*, vol. 86, no. 3, pp. 1430–1436, Feb. 2014.

[40] B. A. Prabowo, L.-C. Su, Y.-F. Chang, H.-C. Lai, N.-F. Chiu, and K.-C. Liu, "Performance of white organic light-emitting diode for portable optical biosensor," *Sens. Actuators B, Chem.*, vol. 222, pp. 1058–1065, Jan. 2016.

[41] R. S. Babu, H. R. Colenso, G. J. Gouws, B. Auguie, and C. P. Moore, "Development of a surface-plasmon resonance sensor testbed for bimetallic sensors," in *Proc. IEEE Int. Instrum. Meas. Technol. Conf. (I2MTC)*, May 2019, pp. 1–6.

[42] S. Long et al., "Grating coupled SPR sensors using off the shelf compact discs and sensitivity dependence on grating period," *Sensors Actuators Rep.*, vol. 2, no. 1, Nov. 2020, Art. no. 100016.

[43] A. Ciesielski, L. Skowronski, W. Pacuski, and T. Szoplik, "Permittivity of Ge, Te and Se thin films in the 200–1500 nm spectral range. Predicting the segregation effects in silver," *Mater. Sci. Semicond. Process.*, vol. 81, pp. 64–67, Jul. 2018.

[44] A. D. Rakic, A. B. Djurišic, J. M. Elazar, and M. L. Majewski, "Optical properties of metallic films for vertical-cavity optoelectronic devices," *Appl. Opt.*, vol. 37, no. 22, pp. 5271–5283, Aug. 1998.

[45] K. M. McPeak et al., "Plasmonic films can easily be better: Rules and recipes," *ACS Photon.*, vol. 2, no. 3, pp. 326–333, 2015.

[46] P. E. Ciddor, "Refractive index of air: New equations for the visible and near infrared," *Appl. Opt.*, vol. 35, no. 9, pp. 1566–1573, 1996.

[47] C. Y. Tan and Y. X. Huang, "Dependence of refractive index on concentration and temperature in electrolyte solution, polar solution, nonpolar solution, and protein solution," *J. Chem. Eng. Data*, vol. 60, no. 10, pp. 2827–2833, 2015.

[48] A. Michelson, *Studies in Optics*. Chicago, IL, USA: The Univ. Chicago Press, 1927.

[49] A. Kolomenski, A. Kolomenskii, J. Noel, S. Peng, and H. Schuessler, "Propagation length of surface plasmons in a metal film with roughness," *Appl. Opt.*, vol. 48, no. 30, pp. 5683–5691, Oct. 2009.

[50] L. M. Brekhovskikh, *Waves in Layered Media*, 2nd ed. New York, NY, USA: Academic, 1980.

[51] W. M. Yunus and A. B. Rahman, "Refractive index of solutions at high concentrations," *Appl. Opt.*, vol. 27, no. 16, pp. 3341–3343, Aug. 1988.

[52] B. W. Grange, W. H. Stevenson, and R. Viskanta, "Refractive index of liquid solutions at low temperatures: An accurate measurement," *Appl. Opt.*, vol. 15, no. 4, pp. 858–859, Apr. 1976.

[53] H. R. Colenso et al., "Comparison of seed layers for smooth, low loss silver films used in ultraviolet-visible plasmonic imaging devices," *Thin Solid Films*, vol. 656, pp. 68–74, Jun. 2018.

[54] M. Schøler and R. J. Blaikie, "Simulations of surface roughness effects in planar superlenses," *J. Opt. A, Pure Appl. Opt.*, vol. 11, no. 10, Aug. 2009, Art. no. 105503.

[55] M. Todeschini, A. B. da Silva Fanta, F. Jensen, J. B. Wagner, and A. Han, "Influence of Ti and Cr adhesion layers on ultrathin Au films," *ACS Appl. Mater. Interface*, vol. 9, no. 42, pp. 37374–37385, Oct. 2017.

[56] P. Lecaruyer, M. Canva, and J. Rolland, "Metallic film optimization in a surface plasmon resonance biosensor by the extended Rouard method," *Appl. Opt.*, vol. 46, no. 12, pp. 2361–2369, Apr. 2007.

[57] X. Jin, J. Lu, P. Liu, and H. Tong, "The electrochemical formation and reduction of a thick AgCl deposition layer on a silver substrate," *J. Electroanal. Chem.*, vol. 542, pp. 85–96, Jan. 2003.

[58] B. Bozzini, G. Giovannelli, and C. Mele, "Electrochemical dynamics and structure of the Ag/AgCl interface in chloride-containing aqueous solutions," *Surf. Coat. Technol.*, vol. 201, no. 8, pp. 4619–4627, Jan. 2007.

[59] J. Song, L. Wang, A. Zibart, and C. Koch, "Corrosion protection of electrically conductive surfaces," *Metals*, vol. 2, no. 4, pp. 450–477, Nov. 2012.

[60] D. R. Lide, *CRC Handbook of Chemistry and Physics*. Boca Raton, FL, USA: CRC Press, 2004.

[61] F. Miculescu, I. Jepu, C. Porosnicu, C. P. Lungu, M. Miculescu, and B. Burhala, "A study on the influence of the primary electron beam on nanodimensional layers analysis," *Dig. J. Nanomater. Biostruct.*, vol. 6, no. 1, pp. 307–317, Mar. 2011.

[62] H. Raether, G. Hohler, and E. A. Niekisch, *Surface Plasmons on Smooth and Rough Surfaces and on Gratings*, vol. 111, 1st ed. Cham, Switzerland: Springer, 1988.

[63] E. Fontana and R. H. Pantell, "Characterization of multilayer rough surfaces by use of surface-plasmon spectroscopy," *Phys. Rev. B, Condens. Matter*, vol. 37, no. 7, pp. 3164–3182, Mar. 1988.

[64] Z. Yang, D. Gu, and Y. Gao, "An improved dispersion law of thin metal film and application to the study of surface plasmon resonance phenomenon," *Opt. Commun.*, vol. 329, pp. 180–183, Oct. 2014.

[65] K. M. Byun, S. J. Yoon, and D. Kim, "Effect of surface roughness on the extinction-based localized surface plasmon resonance biosensors," *Appl. Opt.*, vol. 47, no. 31, pp. 5886–5892, Nov. 2008.

[66] D. V. Nesterenko and Z. Sekkat, "Resolution estimation of the Au, Ag, Cu, and Al single- and double-layer surface plasmon sensors in the ultraviolet, visible, and infrared regions," *Plasmonics*, vol. 8, no. 4, pp. 1585–1595, Dec. 2013.

[67] S. Rodriguez-Mozaz, M. P. Marco, M. J. L. de Alda, and D. Barceló, "Biosensors for environmental applications: Future development trends," *Pure Appl. Chem.*, vol. 76, no. 4, pp. 723–752, Apr. 2004.